NO₂ concentration differences under clear versus cloudy skies and implications for applications of satellite measurements

- 3 Daniel L. Goldberg*,1, M. Omar Nawaz1, Congmeng Lyu2,3, Jian He2,3, Annmarie G. Carlton4, Shobha
- 4 Kondragunta⁵, Susan C. Anenberg¹
- 5 Department of Environmental and Occupational Health, Milken Institute School of Public Health, George
- 6 Washington University, Washington, DC, USA
- 7 2Cooperative Institute for Research in Environmental Sciences, University of Colorado, Boulder, CO, USA
- 8 ³NOAA Chemical Sciences Laboratory, Boulder, CO, USA
- 9 ⁴Department of Chemistry, University of California Irvine, Irvine, CA, USA
- ⁵NOAA NESDIS Center for Satellite Applications and Research, College Park, MD, USA
- *Correspondence to: Daniel L. Goldberg (dgoldberg@gwu.edu)

12 Abstract

1

- 13 Satellite measurements of tropospheric trace gases are often only used when there are few clouds, which screens out
- 14 20 70% of the data, depending on geographic region. While the lack of high-quality column measurements during
- 15 cloudy conditions precludes validation of the satellite data, *in situ* surface measurements and model simulations can
- 16 provide insight on the quantitative understanding of NO₂ during cloudy conditions. Here, we intercompare surface
- observations, meteorological reanalysis (ERA5), satellite measurements (TROPOMI and TEMPO), and a model
- 18 (WRF-Chem) during 2019 over the contiguous U.S. to quantify how NO₂ concentrations are different under clear
- 19 and cloudy skies. We find that in situ surface NO₂ measurements are, on average, +17% larger on all days compared
- 20 to restricting to clear sky days and +36% larger during cloudy days versus clear sky days, with a wide distribution
- 21 based on geographic region and roadway proximity: largest in the Northeast U.S. and smallest in the Southwest U.S.
- 22 and near major roadways. WRF-Chem simulated surface NO₂ between cloudy and clear conditions is on average
- 23 much larger than the observed differences: +59% on cloudy days vs. clear days for the model. This suggests that
- NO₂ in WRF-Chem is more responsive to sunlight and associated photochemistry than in reality. Finally, using *in*
- 25 situ NO₂ matched to provisional TEMPO data, we find the NO₂ differences between cloudy and clear conditions to
- 26 be larger in the afternoon than morning. This study quantifies some of the biases in satellite measurements
- introduced by using only clear-sky data.

1 Introduction

Nitrogen dioxide (NO₂) is an air pollutant that adversely affects the human respiratory system (Health Effects Institute, 2022; Khreis et al., 2017) and can lead to premature mortality (Burnett et al., 2004; M. Z. He et al., 2020). NO2 is also an important precursor for ozone (O₃) and fine particulates (PM_{2.5}), which also have serious health impacts. In urban areas, the majority of ambient NO2 originates from local NOx emissions (=NO+NO2; most NOx is emitted as NO which rapidly cycles to NO₂) during high-temperature fossil fuel combustion (Crippa et al., 2021). Although end-of-pipe controls (Busca et al., 1998; Koltsakis & Stamatelos, 1997) can reduce the amount of NOx emitted from engines and boilers, these technologies do not recover 100% of the NOx generation during combustion. As a consequence, NO₂ accumulates in our atmosphere and many urban areas have NO₂ concentrations that exceed the World Health Organization guideline of 5.3 ppb for an annual average (Anenberg et al., 2022).

Observing local air pollution is typically done by *in situ* surface monitors, which are spaced throughout a region with a higher density of monitors typically in areas of high population density and known pollution sources. In the United States, there are 1012 *in situ* monitoring sites measuring some combination of O₃, PM_{2.5}, NO₂, volatile organic compounds (VOCs), and CO (https://www.epa.gov/aqs). While the U.S. monitoring network is more comprehensive than most other countries (Martin et al., 2019), 79% of U.S. counties lack a single monitor and an additional 10% of counties have only a single monitor, leaving only 11% of U.S. counties with more than 1 monitor (Sullivan & Krupnick, 2018). Although a robust and accurate ground-monitoring network is needed, the high operating cost of these instruments can be an important barrier (Kelly et al., 2017). Spatial gaps remain in-between the regulatory monitors, and sometimes these monitors are inadequate for understanding the true ambient air pollution exposure of most U.S. residents, especially those that live and/or work several miles away from a regulatory monitor. Satellite data provide a way to fill in the gaps of the *in situ* monitoring network. Methodologies to obtain robust surface air pollutant measurement data from satellite instruments have improved dramatically in the past ten years (Bechle et al., 2015; Cao, 2023; Ghahremanloo et al., 2021, 2023; Larkin et al., 2023; Nawaz et al., 2025; Shetty et al., 2024; W. Sun et al., 2024).

NO₂ can be observed by remote sensing instruments due to its unique spectroscopic features (Vandaele et al., 1998). The Tropospheric Monitoring Instrument (TROPOMI) (Veefkind et al., 2012) has been measuring column amounts of NO₂ pollution up to 7 × 3.5 km² before 6 August 2019 and up to 5.5 × 3.5 km² spatial resolution (van Geffen, 2016) since 6 April 2019. Because of TROPOMI's higher spatial resolution over predecessor instruments, such as the Ozone Monitoring Instrument (OMI) (24 × 13 km² at nadir) (Levelt et al., 2018), TROPOMI has ~50 daily satellite pixel measurements within a typical city (~1000 km²) during clear skies, while OMI may have only 1-3 daily measurements within the borders of each city. This increased measurement capacity within a city allows us to discern spatial variability undetectable by previous instruments. Further, the data from the satellite instruments can be downscaled using a process called oversampling (de Foy et al., 2009; K. Sun et al., 2018), which re-grids the irregular satellite pixels to a standard and higher spatial resolution. The spatial resolution is thus effectively increased at the expense of the temporal resolution.

63 NO₂ satellite measurements are of the tropospheric column. In many cases, NO₂ column measurements are strongly 64 correlated with the spatial patterns of surface NO₂ concentrations (Acker et al., 2025; Harkey & Holloway, 2024; Kim 65 et al., 2024) and surface NOx emissions (Goldberg et al., 2024). For TROPOMI, studies have shown a strong 66 correlation between tropospheric column measurements and collocated surface NO_2 for both the 13:30 average (r^2 = 67 0.67) and the 24-hour average ($r^2 = 0.68$) (Goldberg et al., 2021; Kerr et al., 2023). However, there are rare instances in which NOx emissions and NO2 enhancements stay aloft and do not affect the surface; these are often situations 68 69 associated with lightning NOx (Nault et al., 2017), wildfire NOx (Jin et al., 2021; Lin et al., 2024), and aircraft NOx 70 (Maruhashi et al., 2024). In these instances, it can be difficult to determine if the column NO₂ enhancements are also 71 leading to surface NO2 enhancements. These misinterpretations are more likely to occur over rural regions and/or 72 individual days, as upper-tropospheric NO2 enhancements near urban regions often dwarf NO2 enhancements within 73 the boundary layer especially over monthly or longer timescales (Goldberg et al., 2022). 74 Satellite measurements of trace gases are typically only used when there are few or no clouds; this is often referred 75 to as the clear-sky bias of satellite data. In the U.S., this results in 20 - 70% of the satellite data being filtered out 76 depending on geographic region. The clear-sky bias affects NO2 moreso than other trace gases (such as CO and 77 CH₄) because NO₂ is very photochemically active in the presence of strong sunlight; its effective lifetime during 78 summer daytime is 2 – 7 hours (F. Liu et al., 2016) and conversely can be up to 30 hours during winter daytime 79 (Kenagy et al., 2018). The speed at which it transforms into other chemical species is determined by the irradiation, 80 ambient temperature, and oxidation environment (Laughner & Cohen, 2019; Shah et al., 2020). More specifically, 81 strong irradiation creates the OH radical which can react with NO₂ to create HNO₃ – a major terminal sink of NO₂ – 82 and also accelerates the photolysis of NO2 into NO and O(3P) leading to an accumulation of O3 in the presence of 83 VOCs; without VOCs, NO2 cycles more rapidly to NO. Warm temperatures increase biogenic VOC emissions and 84 VOC can react with NO₂ directly to create organic nitrates (e.g., peroxyacetyl nitrates and alkyl nitrates) (Zare et al., 85 2018) which act as a temporary sink of NO₂. Another daytime terminal sink for NO₂ is dry deposition; while this 86 removal mechanism is often secondary to photochemical loss in urban environments and is not directly affected by 87 sunlight, it is indirectly affected as cloudy conditions are often associated with increased relative humidity and 88 shallower boundary layer depths, both of which increase dry deposition. Therefore, increased NO₂ dry deposition in 89 cloudy conditions could offset some of the decreased NO₂ photochemical loss rates. The net result is that NO₂ 90 concentrations are typically larger during cloudy conditions (Geddes et al., 2012). 91 However, outside of the Geddes et al. (2012) study, little has been done to observationally quantify the bias of NO₂ 92 being larger during cloudy conditions particularly because there are no column measurements to validate the satellite 93 during cloudy conditions. With that said, there are surface in situ measurements during cloudy conditions that can 94 give us an idea of how the clear-sky bias may affect the estimate of surface concentrations. In this project, we 95 intercompare surface observations, meteorological reanalysis (ERA5), satellite measurements (TROPOMI and 96 TEMPO), and a model (WRF-Chem) under clear and cloudy skies to better quantify the amount of surface and 97 column bias of NO₂ concentrations that is being introduced when clouds are screened from the satellite data. Our

analysis is focused on the United States during 2019 due the high density of in situ monitors and availability of high-

resolution regional chemical transport models. The motivation of this project is two-fold: 1) to determine what the scientific community may be missing when excluding clouds from TROPOMI-based NO₂ analyses and 2) to understand how geostationary NO₂ satellite measurements may be affected by such a bias and potentially partially remediate such a bias.

2 Methods

2.1 EPA AQS Data

Hourly *in situ* NO₂ measurements were obtained from the pre-generated EPA Air Quality System (AQS) database: https://aqs.epa.gov/aqsweb/airdata/download_files.html. These routine measurements are operated and maintained by various state and federal agencies. 91% of the "NO₂" measurements in 2019 were acquired through a chemiluminescence technique which converts NO₂ and some NO_y species – such as alkyl nitrates, peroxynitrates (PAN), and nitric acid (HNO₃) – to NO using a heated molybdenum converter, and the NO is measured by quantifying the luminesce of NO when reacted in excess O₃ (Dickerson et al., 2019). Lamsal et al. (2008) suggested a correction factor, Equation 1, for converting midday chemiluminescence NO₂* measurements to NO₂ using modelled information of PAN and HNO₃.

Typically, correction factors are in the range of \sim 1.0 for fresh urban plumes and can be as large as \sim 3.0 for rural areas during summer, with averages typically in the 1 – 1.5 range for moderate and very polluted regimes, and are important to use for model vs. monitor intercomparisons (Kuhn et al., 2024; Lamsal et al., 2008; Poraicu et al., 2023). Other methods to measure *in situ* NO₂ include Cavity Attenuated Phase Shift (Kebabian et al., 2008) and Laser Induced Fluorescence (Thornton et al., 2000), but these methods are less common (9% of all NO₂ monitors in 2019).

Annual and seasonal averages at 13:30 local standard time (between 13:00 – 14:00) of the *in situ* data were considered valid and used if more than 75% of the days of the year/season had valid data. There were 449 monitoring locations in 2019 in the U.S. that achieved these criteria for an annual average, which equates to 1 monitor per ~730,000 U.S. residents. For the baseline analysis, we further remove data from the 75 monitoring locations (17% of the locations) that are classified as "near-road" by the EPA, which means that they are installed within 20 m from major interstates since these *in situ* measurements are not representative of a ~20 km² satellite pixel measurement; we include the "near-road" NO₂ monitoring data in sensitivity analyses. NO₂ measurements between cloudy and clear-sky days are intercompared using the normalized mean change (NMC) as described in Equation 2, where \bar{x} and \bar{y} are means of the two datasets being analyzed.

$$NMC(\%) = 100 \times \left(\frac{\bar{y} - \bar{x}}{\bar{x}}\right) \tag{2}$$

2.2 Satellite NO₂ Instruments

131

132 NO₂ slant column densities are derived from radiance measurements in the 405 – 465 nm spectral window of the UV-133 VIS-NIR spectrometer (van Geffen et al., 2021). Satellite instruments observe NO2 by comparing observed spectra 134 with a reference spectrum to derive the amount of NO₂ in the atmosphere between the instrument and the surface; this 135 technique is called differential optical absorption spectroscopy (DOAS) (Platt, 1994). Tropospheric vertical column 136 density data, which represent the vertically integrated NO2 concentrations between the surface and the tropopause, are 137 then calculated by subtracting the stratospheric portion and then converting the tropospheric slant column to a vertical column using an air mass factor (AMF) (Boersma et al., 2011). The AMF is a unitless quantity used to convert the 138 139 slant column into a vertical column and is a function of the satellite viewing angles, solar angles, the effective cloud 140 radiance fraction and pressure, the vertical profile shape of NO₂ provided by a chemical transport model simulation, 141 and the surface reflectivity (Lorente et al., 2017; Palmer et al., 2001).

142 **2.2.1 TROPOMI**

- 143 TROPOMI was launched by the European Space Agency (ESA) on 13 October 2017, and data from the instrument
- became available on 30 April 2018, after an approximately 6-month calibration period. The satellite follows a sun-
- synchronous, low-earth (825 km) orbit with an equator overpass time of approximately 13:30 local solar time.
- 146 TROPOMI measures total column amounts of several trace gases: NO2, HCHO, O3, CO, CH4, among others. At nadir,
- pixel sizes are $3.5 \times 7 \text{ km}^2$ (modified to $3.5 \times 5.5 \text{ km}^2$ on August 6, 2019) with the edges having slightly larger pixels
- sizes (~14 km wide) across a 2600 km swath, equating to 450 rows (van Geffen et al., 2020).
- For our analysis we use the TROPOMI NO₂ version 2.4 (V2.4) re-processed algorithm during Jan 1, 2019 Dec 31,
- 150 2019. We also conducted a sensitivity study using the version 2.3.1 (V2.3.1) algorithm. The TROPOMI NO₂ V2.4
- product has a documented median low bias of -34.8% in moderately polluted locations (when NO₂ measurements are
- between 3 14 x 10¹⁵ molec/cm²) when compared to a MAX-DOAS network (Lambert et al., 2023). Some of this low
- bias is due to the operational AMF which uses a $1^{\circ} \times 1^{\circ}$ model to assume vertical shape profiles; when vertical shape
- profiles from a regional model are instead used, the bias decreases to between -1% and -23% (Nawaz et al., 2024,
- Judd et al., 2020, Tack et al., 2021). Prior work has demonstrated a strong correlation between TROPOMI NO₂ column
- measurements and NO₂ surface concentrations in urban areas (Demetillo et al., 2020; Dressel et al., 2022; Goldberg
- et al., 2021; Nawaz et al., 2025). For our baseline, we screened TROPOMI pixels for quality assurance flag values
- greater than 0.75, and conduct a sensitivity analysis of filtering only with a cloud radiative fraction filter of 0.5. The
- 159 cloud radiative fraction is calculated from the O₂ A-band using the FRESCO-S algorithm. Due to differences in
- wavelength between the O₂ A-band and the NO₂ retrieval window, the cloud fraction retrieved in the O₂ A-band is not
- exactly representative for the cloud fraction in the NO₂ window, but it is similar.
- 162 The filtered data were re-gridded to a 0.01° × 0.01° resolution, to create a custom "Level-3" data product (Goldberg
- et al., 2021) during cloud-free and cloudy conditions. Single pixel TROPOMI tropospheric vertical column NO₂
- uncertainties have been quantified to be between 25 50% under clear skies and this uncertainty is dominated by

- uncertainty in the tropospheric air mass factor (Glissenaar et al., 2025; S. Liu et al., 2021; Rijsdijk et al., 2025);
- uncertainties of measurements with cloud fractions > 0.5 are larger. Oversampled NO₂ measurements over monthly
- and annual timeframes (10s 100s of measurements) have a smaller amount of uncertainty, approximately 10 20 %
- depending on location and season (Glissenaar et al., 2025).

2.2.2 TEMPO

169

184

192

- 170 TEMPO was launched by SpaceX on 7 April 2023 and is hosted on Maxar Intelsat 40e. Data from the instrument
- became available on 2 August 2023, after an approximately 4-month dry-out, cool-down, and calibration period. The
- satellite is in geostationary orbit centered over the United States with north-south coverage extending from Mexico
- 173 City (~17°N) to the Canadian Oil Sands (~58°N) and east-west coverage from Puerto Rico to the Pacific coast.
- 174 TEMPO operationally measures total column amounts of NO₂, HCHO, and O₃ with additional products forthcoming.
- At nadir, pixel sizes are 4.75 × 2 km² with the North-east and North-west edges having slightly larger pixels sizes.
- 176 The instrument observes the full east-west swath approximately once every hour.
- 177 For our analysis we use the TEMPO NO₂ version 3 algorithm during 2 Aug 2023 31 Aug 2024. The data was filtered
- to include pixels only where the effective cloud fractions are less than 0.15 and the main data quality flags are equal
- to 0. The filtered data was re-gridded to a 0.01° × 0.01° resolution, to create a custom "Level-3" data product (Goldberg
- et al., 2021) during cloud-free and cloudy conditions. Single pixel TEMPO tropospheric vertical column NO2
- uncertainties can be assumed to be similar to the uncertainty of TROPOMI measurements (Glissenaar et al., 2025),
- which are between 25 50% under clear skies for individual pixels, and 10 20% for oversampled averages; future
- work will better quantify the uncertainties of TEMPO NO₂ measurements.

2.3 ERA5 Re-analysis

- We intercompare the cloud radiative fractions from TROPOMI to the ERA5 re-analysis (Hersbach et al., 2020) of
- total cloud fractions in the early afternoon (18Z for Eastern Time, 19Z for Central Time, 20Z for Mountain Time, 21Z
- for Pacific Time), which approximates the overpass time of TROPOMI over the contiguous United States. The ERA5
- total cloud fraction is a unitless quantity representing how much of a grid cell is covered by a cloud (e.g., condensed
- water vapor) at any vertical level of the atmosphere and does not differentiate between the optical properties of those
- 190 clouds. The ERA5 re-analysis data are reported at a 0.25° × 0.25° spatial resolution and the cloud fractions are
- interpolated, using bilinear interpolation, to the 0.01° × 0.01° oversampled TROPOMI NO₂ grid.

2.4 WRF-Chem

- 193 The Weather Research and Forecasting with Chemistry (WRF-Chem) model was run at 12 km × 12 km over the
- 194 Continental U.S. for all days of 2019: 1 January 2019 31 December 2019 as described in He et al. (2024). For
- anthropogenic emissions, the Fuel-based Inventory of Vehicle Emissions (FIVE) was used to provide on-road and off-
- road mobile emissions, the Fuel-based Oil and Gas (FOG) inventory was used for emissions associated with oil and
- natural gas production, power plant emissions were provided by Continuous Emissions Monitoring Systems (CEMS),

and all other anthropogenic emissions were obtained from the 2014 or 2017 National Emissions Inventory (NEI). Biogenic emissions were estimated using Biogenic Emissions Inventory System (BEIS) version 3.13. Gas-phase chemistry was from the RACM_ESRL_VCP scheme. Boundary conditions were provided from the Realtime Air Quality Modeling System (RAQMS, http://raqms-ops.ssec.wisc.edu/) developed by the University of Wisconsin-Madison. The cloud fractions used in this project are from the total cloud fraction "CLDFRA" variable.

3 Results

3.1 CONUS Cloud Patterns

We first conduct an analysis of cloud patterns across the contiguous United States, and inter-compare clear-sky days estimated by TROPOMI, the ERA5 re-analysis, and the WRF-Chem model (Figure 1). For TROPOMI, we define clear skies as the percentage of days with qa_value > 0.75, which almost exclusively filters based on cloud fractions <0.5; cloud-free snow-covered scenes typically have a qa_value > 0.75 (Eskes et al., 2022). For ERA5 and WRF-Chem, we define clear skies as the percentage of days with the total cloud fractions <0.5. ERA5 and WRF-Chem have similar clear-sky spatial patterns as TROPOMI but show systematically lower amounts of clear-skies by 8%. The small systematic difference between TROPOMI and ERA5 when filtering for cloud fractions at 13:30 is likely driven by how optically thin cirrus-like clouds are handled; for TROPOMI these are being observed based on optical properties and therefore optically thin clouds are not assumed to be a cloud, whereas in weather models (ERA5 and WRF-Chem) these are being computed as vertical layers in the atmosphere with condensed water vapor. Overall, there is very strong agreement between the three datasets in the estimation of clouds giving us confidence that TROPOMI, ERA5, and WRF-Chem are all good estimators of daily clear-sky amounts.

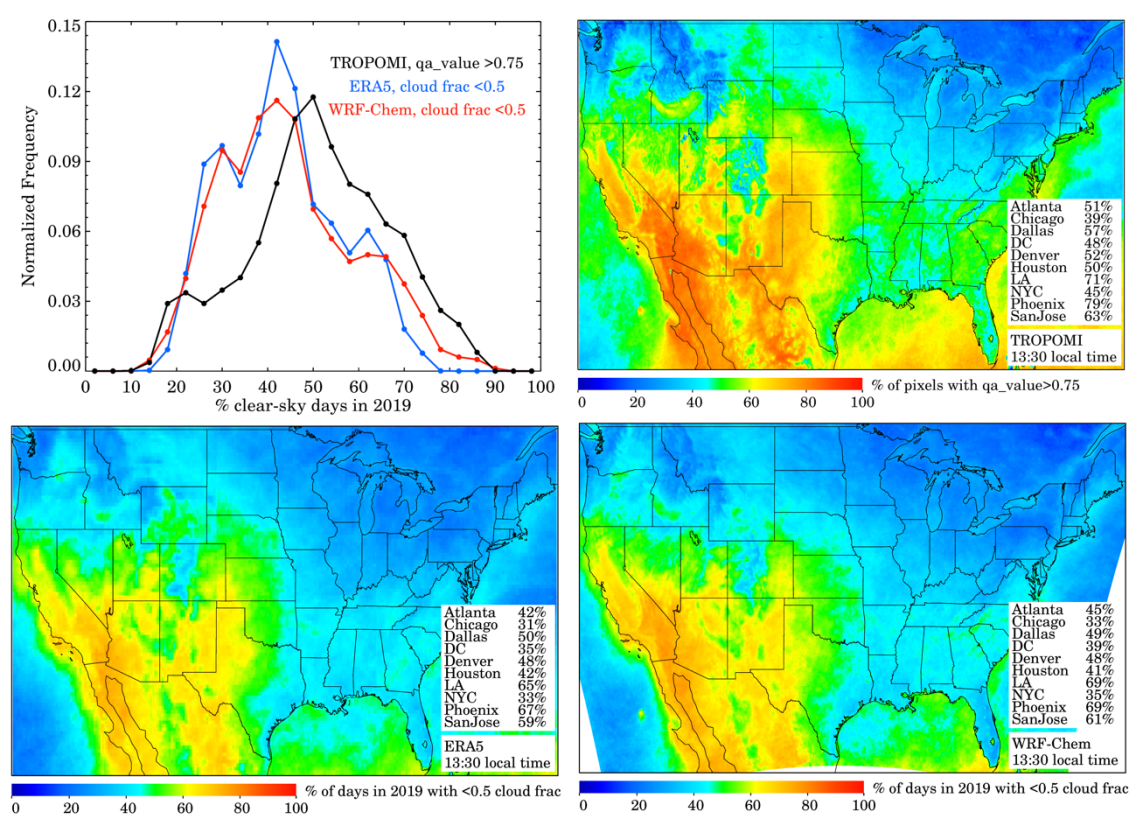


Figure 1. Percentage of clear-sky days over the contiguous U.S. during 2019 from the TROPOMI NO₂ V2.4 product, ERA5 re-analysis, and WRF-Chem. (Top left) Normalized frequency diagram of the binned percentage of clear sky days for the three products. (Top right) Percentage of days in which the qa_value of the TROPOMI NO₂ V2.4 measurement was greater than 0.75. (Bottom left) Percentage of days in which the total cloud cover (tcc) from the ERA5 was less than 0.5. (Bottom right) Percentage of days in each grid cell in which the total cloud fraction from the WRF-Chem was less than 0.5

For the remainder of this project, we define "clear sky" based on the TROPOMI NO₂ retrieval and use days with observations exceeding a qa_value of 0.75. According to TROPOMI – which is the only true observational dataset – the Southwest U.S. has the most amount of clear-sky days per year (~80% of days at 13:30 local time), while the interior Northeast U.S. and coastal Northwest has the fewest (~30% of days at 13:30 local time). The major U.S. city with the most clear-sky days is Phoenix (79% of days), while the major U.S. city with the least clear-sky days is Seattle (29% of days).

Annualized spatial cloud patterns are similar throughout the daylight hours with marginally more clear skies in the morning hours especially in the eastern U.S (Figure S1). Despite this, clouds are often transient, and there are opportunities to observe a clear sky measurement at a different hour of the day if the 13:30 observation is obstructed by clouds. In Figure 2, we demonstrate that between 68% - 93% of days have a clear sky measurement during any hour of the daytime as compared to the 33 - 69% range at 13:30.

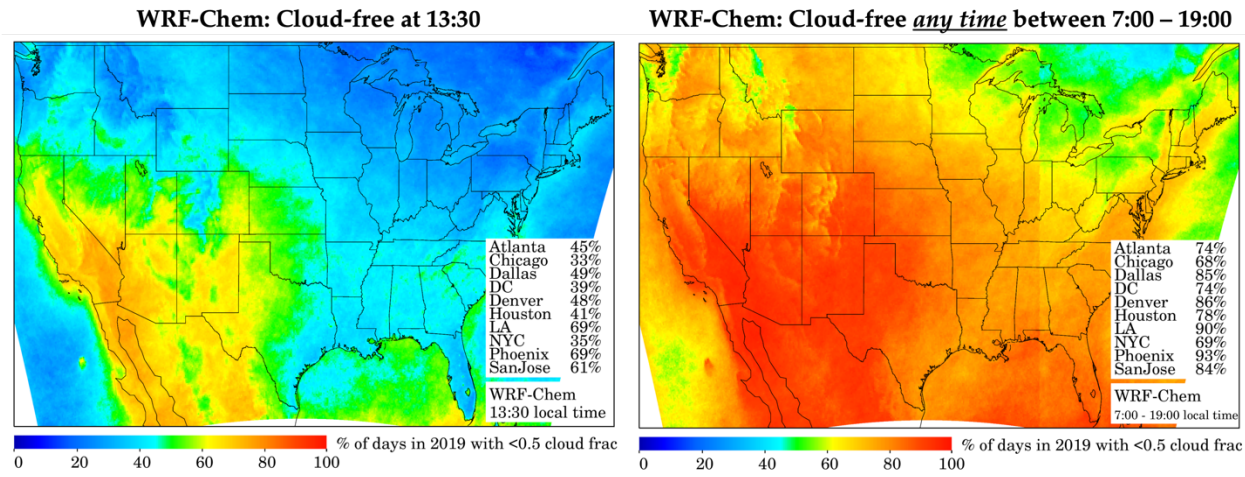


Figure 2. Percentage of days over the contiguous U.S. during 2019 with cloud fractions less than 0.5 as simulated by WRF-Chem at various local times: (Left) 13:30, (Right) any time between 7:00 - 19:00.

3.2 Surface NO2: Clouds vs. No Clouds

We then link whether TROPOMI is observing a clear sky or not (i.e., $qa_value > 0.75$) to the daily *in situ* ground-level NO₂ observations to determine how clouds are affecting surface NO₂ concentrations (hereafter referred to as surface NO₂). In Figure 3, we show that surface NO₂ at 13:30 local time is +12.9% larger (NMC = normalized mean change) [-3.8% (10^{th} percentile), +32.1% (90^{th} percentile)] on days with clouds at 13:30 compared to the annualized 13:30 average when all days of data are included. We also note the very strong correlation between the NO₂ on cloudy days and all days, which suggests that the presence of clouds drives a systematic change from the mean rather than a random change. We next show that the NO₂ during the average of all days is +17.2% larger [-1.8%, +38.7%] than on days with only clear skies. The +17.2% value is our estimate of the difference of annualized surface-based NO₂ at 13:30 on all days as compared to only clear sky days. We further show that surface NO₂ at 13:30 is +36.0% larger [-6.1%, +72.9%] on days with clouds compared to days with clear skies.

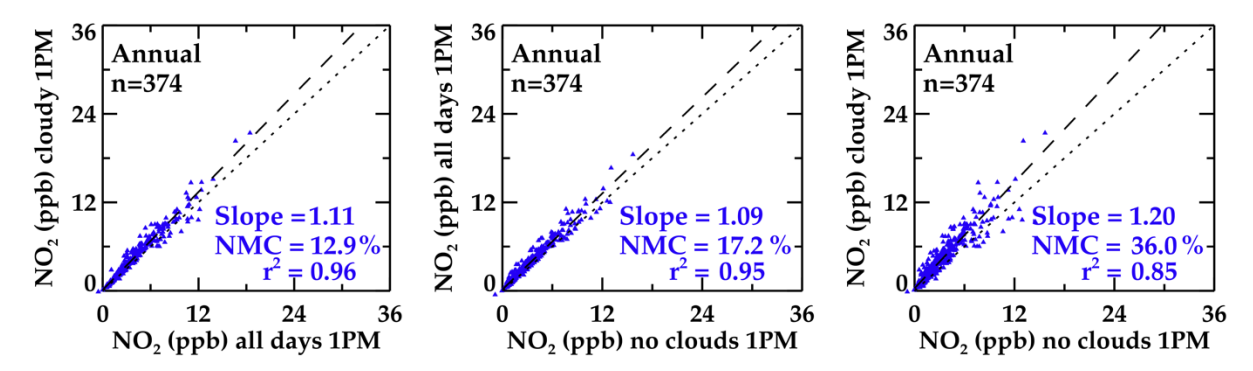


Figure 3. Scatterplots intercomparing annualized surface NO₂ from the EPA AQS at 13:30 local time during all days, cloudy days, and no cloud days. (Left) Annualized surface NO₂ during cloudy days compared to annualized surface NO₂ during all days. (Center) Annualized surface NO₂ during all days compared to annualized surface NO₂ during no cloud days. (Right) Annualized surface NO₂ during cloudy days compared to annualized surface NO₂ during no cloud. A "cloudy" vs "no cloud" day is determined via the qa_value of 0.75 from the TROPOMI NO₂ V2.4 product.

The difference in surface NO₂ between cloudy and clear sky days can vary dramatically based on geographic region and proximity to a major roadway (Table 1). For the purposes of the sensitivity study, we focus on the cloudy versus no cloud days, while the directional changes of "cloudy versus all days" and "all days versus no clouds" values are similar (Tables S1 & S2).

Table 1. Slope, r², Normalized Mean Change (NMC), and number of sites of the "cloudy vs. no clouds" bias by further filtering out AQS data using various additional sensitivity analyses. Tables S1 & S2 show the sensitivity analyses for the "cloudy vs. all days" bias, and "all days vs. no clouds" bias respectively.

			Normalized Mean	# sites of monitoring
	Slope	r ²	Change (%)	sites used
Baseline (V2.4)	1.20	0.85	+36.0%	374
V2.3.1	1.18	0.86	+40.4%	374
V2.4 crf<0.5	1.25	0.83	+80.8%	373
V2.4 all sites	1.05	0.90	+32.7%	449
V2.4 near road only	0.89	0.84	+15.9%	76
V2.4 no chemiluminescence	1.20	0.87	+53.1%	26
V2.4 Summer only	1.17	0.86	+23.8%	366
V2.4 Winter only	1.14	0.82	+27.8%	373
V2.4 Spring only	1.28	0.88	+31.9%	364
V2.4 Fall only	1.07	0.77	+30.9%	359
V2.4 North only	1.31	0.89	+41.5%	217
V2.4 South only	0.98	0.82	+28.5%	157
V2.4 NorthEast only	1.36	0.93	+61.7%	106
V2.4 SouthEast only	1.27	0.94	+33.8%	73
V2.4 NorthWest only	1.12	0.88	+22.2%	111
V2.4 SouthWest only	0.91	0.79	+23.9%	84
V2.4 lowPopDensity only	1.34	0.86	+36.3%	216
V2.4 highPopDensity only	1.13	0.76	+37.5%	167
V2.4 lowRoadDensity only	1.19	0.82	+33.6%	216
V2.4 highRoadDensity only	1.18	0.80	+40.8%	165

First, we find that NO₂ during cloudy days is larger in the northern U.S. (+41.5%) than the southern U.S. (+28.5%) and largest in the Northeast U.S (+61.7%) (Figure 4); for this analysis, 37°N is the dividing latitude between North and South, 100°W is the dividing longitude between East and West. Although the calculated cloudy versus no cloud change is independent of the number of days of clear-skies, areas of perpetually cloudy skies also have cooler temperatures and shallower boundary layers which could cause much larger NO₂ on cloudy days. Interestingly, the Phoenix and Salt Lake City areas – two areas with large number of days with clear skies – also have a relatively large difference between cloudy and clear sky days demonstrating that the bias is independent of the number of days with clear skies. However, the *annualized* difference between cloudy and clear sky days in the Southwest U.S. is modest (+4.8%) (Table S1) because there are fewer individual days affected by clouds. Approximately 13% of monitoring sites, mostly concentrated in the Los Angeles and San Diego areas, have lower NO₂ on cloudy days, and this may be driven by enhanced westerly winds on cloudy days bringing in cleaner marine air more than offsetting the photochemically driven larger NO₂ on cloudy days. Overall, while there are a few locations with lower NO₂ on cloudy days, 87% of locations exhibit larger NO₂ on cloudy days and this is driven by the slower photochemistry on these days.

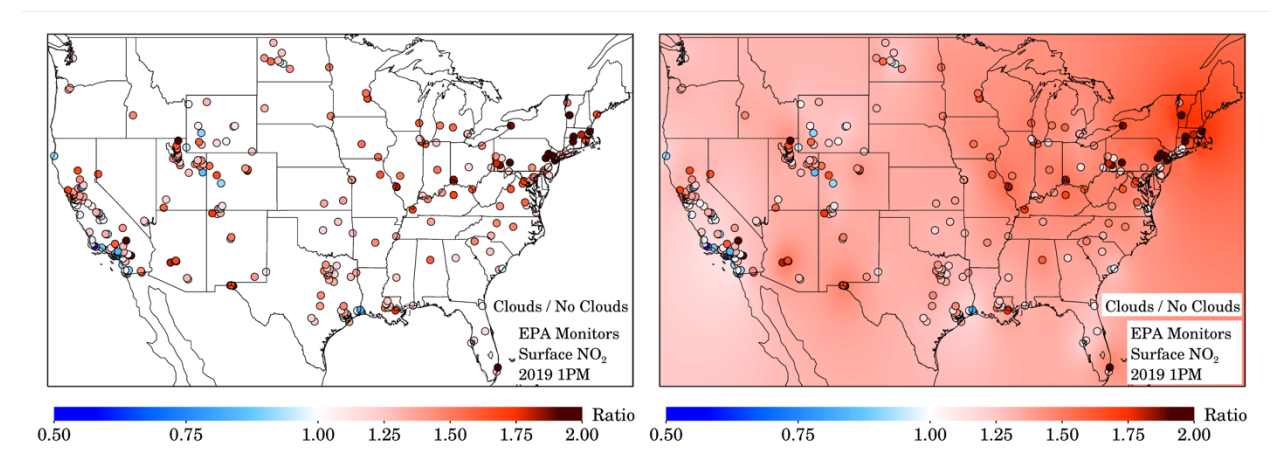


Figure 4. (Left) Ratio of the annualized surface NO₂ during cloudy and no cloud days at the EPA AQS sites not classified as "near-road". (Right) Same image but with an inverse distance weighting underlaid to infer geographic distribution of the ratio.

Proximity to roadways and large sources of NOx is another driver of whether a location will experience a small (but larger) difference in NO₂ on cloudy and clear sky days. For areas in close proximity to roadways (i.e., the near-road sites) (n=76), the difference in NO₂ between cloudy and clear sky days is weaker: a smaller positive change (+15.9%) and only 77% of sites displaying a positive mean change, which is less than the difference at all other NO₂ monitoring locations (+36.0%).

We find that seasonal effects on the differences in NO₂ between cloudy and clear days are modest. The NO₂ on cloudy days in the Spring is largest and marginally smaller in other seasons. Other factors that were not associated with strong changes to the differences in NO₂ between cloudy and clear days bias are: the version of the TROPOMI NO₂ algorithm,

whether the site was using a chemiluminescence or Cavity Attenuated Phase Shift measurement technique, and population / roadway density within a 0.5° radius.

3.3 TROPOMI NO2: Clouds versus No Clouds

We then compare TROPOMI NO₂ measurements under varying sky conditions. For this exercise, we filter the TROPOMI NO₂ data strictly based on cloud radiative fraction (crf). Although it is recommended for most applications to use data when the crf <0.5, sometimes measurements are usable in the presence of optically thick clouds (i.e., crf >0.5). In Figure 5, we average TROPOMI NO₂ measurements below and above a crf = 0.5 threshold to gain an understanding of how TROPOMI column NO₂ measurements intercompare in the presence and lack of optically thick clouds. In the figure we show the tropospheric vertical columns on the top row, and tropospheric slant columns in the middle row, which have been interconverted using the tropospheric air mass factor shown on the bottom row. As discussed in Section 2.2.1, the tropospheric air mass factor can be a large source of uncertainty when calculating tropospheric vertical columns from slant columns (Glissenaar et al., 2025; S. Liu et al., 2021; Rijsdijk et al., 2025).

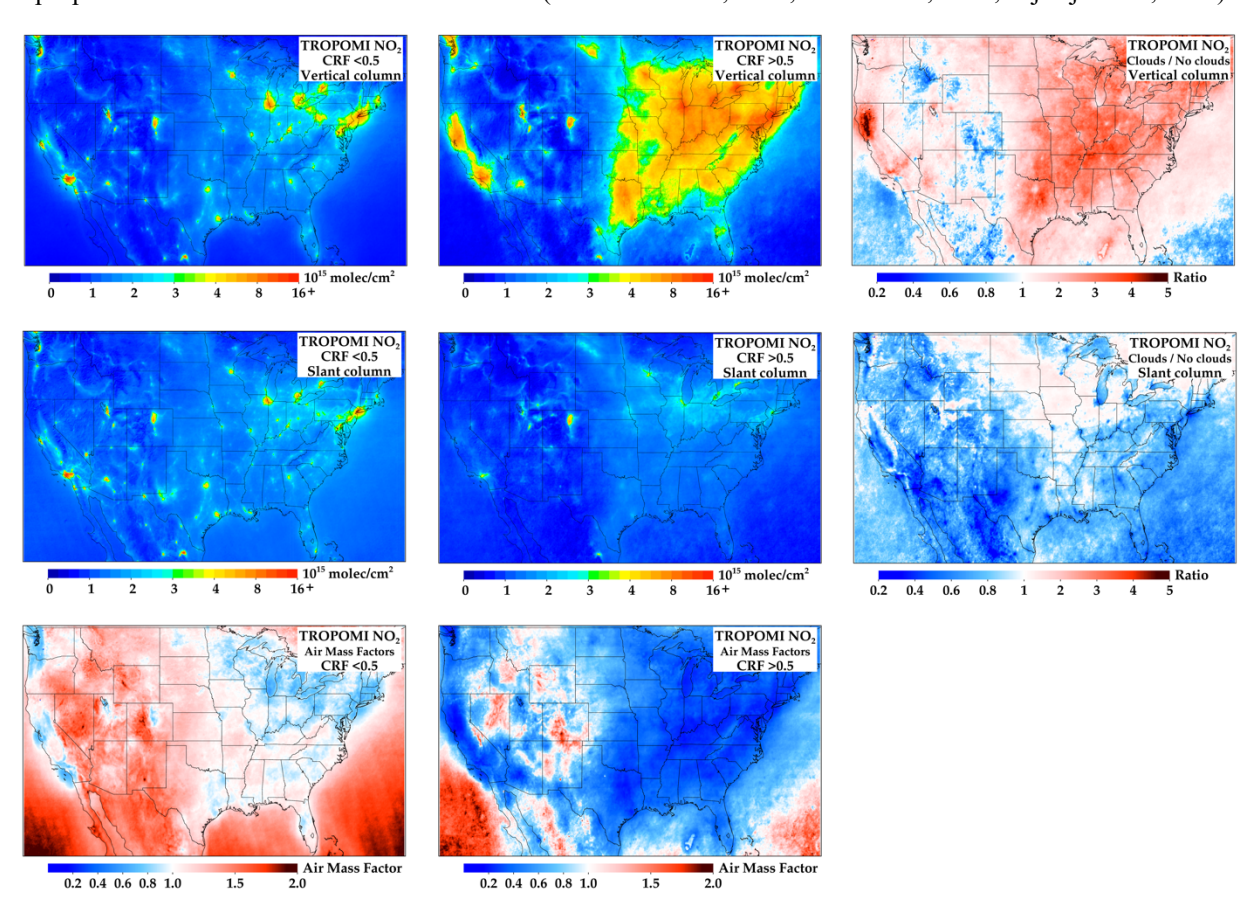


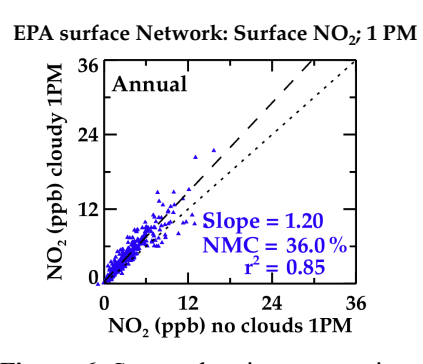
Figure 5. (Left column) Annual 2019 TROPOMI NO₂ filtered using only a cloud radiative fraction (crf) filter less than 0.5. (Center column) Annual 2019 TROPOMI NO₂ filtered using only a crf filter greater than 0.5. (Right column) Ratio between the two annual averages. (Top row) Vertical tropospheric column NO₂ data. (Center row) Slant tropospheric column NO₂ data. (Bottom row) Tropospheric air mass factors.

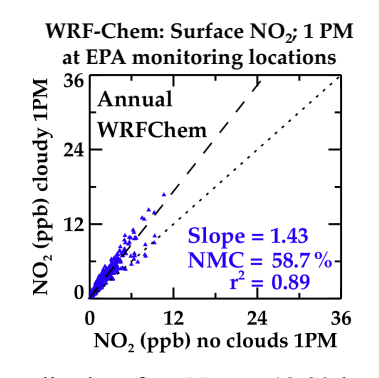
In Figure 5, we demonstrate that the vertical column NO₂ spatial patterns in the presence of clouds are much different in magnitude than the slant column NO₂ whereas the vertical column NO₂ spatial patterns in the absence of clouds are similar to the slant column NO₂. This is primarily driven by the assumed vertical shape profiles in the model. During measurements when the crf >0.5 as compared to measurements when crf <0.5, the model is "filling in" the missing NO₂ and causing small air mass factors as shown. This is primarily because sensitivity to the surface concentrations is altered (lower) in the slant column measurement in the presence of clouds. Also, during measurements when the crf >0.5, the uncertainty of the TROPOMI vertical column measurements rises, and this is driven by the difficulty in calculating the air mass factor in the presence of clouds; in addition to needing to know the vertical NO₂ profile for its calculation, we also need to know the pressure level and thickness of the clouds. Such errors can generate nonlinear responses. This analysis confirms that the assumed air mass factor is the driving factor causing the differences in the tropospheric vertical column NO₂ between clear and cloudy sky days, as the slant tropospheric column NO₂ is smaller during cloudy skies due to a lack of instrument sensitivity to the surface during cloudy conditions. Therefore, special care should be used when interpreting tropospheric satellite measurements in the presence of clouds.

Qualitatively, the ratio of the column NO₂ with and without clouds is spatially similar to the ratio from the AQS analysis – with the largest ratios occurring in the Northeast U.S and smallest ratios occurring in the Southwest U.S. However, quantitatively, the column ratio observed by TROPOMI is much larger in magnitude in the eastern U.S. than the surface ratio observed at the AQS surface sites. It is difficult to determine whether the quantitative magnitude is correct because there are no ground-based instruments to accurately measure column NO₂ in the presence of clouds.

3.4 WRF-Chem NO2: Clouds vs. No Clouds

We then compare the differences in NO₂ between cloudy and clear days observed by the EPA AQS surface network to the differences in NO₂ between cloudy and clear days of surface NO₂ simulated by WRF-Chem. The 13:30 local time differences in NO₂ between cloudy and clear days of surface NO₂ in WRF-Chem (+58.7%) is substantially larger than from the AQS observations (+36.0%) during collocations. This directional change is consistent among all geographic regions suggesting that NO₂ concentrations are too responsive to sunlight in WRF-Chem.





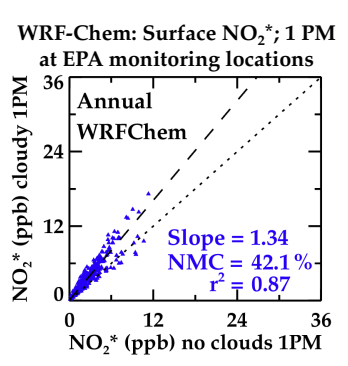


Figure 6. Scatterplots intercomparing annualized surface NO₂ at 13:30 local time during cloudy days vs. no cloud days. (Left) EPA AQS data which is a repeat of Figure 3c. (Center) WRF-Chem collocated with the AQS monitoring sites, and using the WRF-Chem cloud filter in lieu of the TROPOMI cloud filter. (Right) WRF-Chem collocated with the AQS monitoring sites, comparing NO₂* instead of NO₂.

There could be several reasons for this discrepancy. First, 91% of monitors in the EPA monitoring network measure using the chemiluminescence method, NO₂*, which quantifies NO₂ in addition to some fraction of HNO₃. The latter is problematic because the NO₂ + OH → HNO₃ reaction is often the terminal sink for NO₂ during daytime and if HNO₃ is additionally being measured then this would appear to buffer photolytically driven changes. We further conducted a sensitivity test in WRF-Chem and found that the NMC is only +42.1% down from +58.7% when a chemiluminescence correction factor from Equation 1 is used (Figure 6c), indicating that some of the perceived differences between WRF-Chem and EPA monitors could be due to monitor interferences from PAN and HNO3. Second, it is possible that OH concentrations in WRF-Chem are fluctuating too rapidly in the presence of and lack of clouds (Duncan et al., 2024) causing NO₂ to be removed to rapidly in the model. Third, there might be insufficient NO₂ recycling of organic nitrates and/or particulate nitrates in the model which could buffer photolysis-related changes; recent work has suggested that particulate nitrate can meaningfully photolyze back to NO₂ (Sarwar et al., 2024; Shah et al., 2024). Fourth, WRF-Chem may not simulate PBL depth properly and may have different biases during cloudy and clear sky conditions (Hegarty et al., 2018; Kuhn et al., 2024; X. Liu et al., 2023). For example, if the predicted PBL is too shallow during cloudy conditions, this could be a contributing factor to the simulated surface NO₂ bias. Errors in surface jNO₂ do not appear to be a primary driver of the cloudy versus clear sky disagreements as the ¡NO2 values from WRF-Chem seem reasonable as compared to UV-B measurements from the NOAA Surface Radiation Budget (SURFRAD) monitoring network (Figure S4) and is consistent with other work showing small biases in jNO₂ in WRF-Chem (Ryu et al., 2018). Follow-up work will address some of these shortcomings by adding particulate nitrate photolysis into the chemical mechanism and evaluating PBL depths during cloudy conditions using ceilometers.

365 366 367

368

369370

371

345

346347

348

349

350

351

352

353

354

355

356

357

358

359

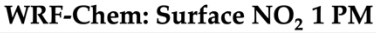
360

361362

363

364

We can then use WRF-Chem as a transfer standard to suggest how column NO₂ may change in relation to the surface NO₂, and we find that the relative change in column NO₂ and surface NO₂ in response to clouds are very similar (Figure 7). This makes intuitive sense because most NO₂ over the contiguous U.S. is located within the boundary layer, and typically clouds (if they exist) are located at the top of the boundary layer. Any sunlight obstructed by clouds will also obstruct the NO₂ both at the surface and in the full boundary layer.



WRF-Chem: Column NO₂ 1 PM

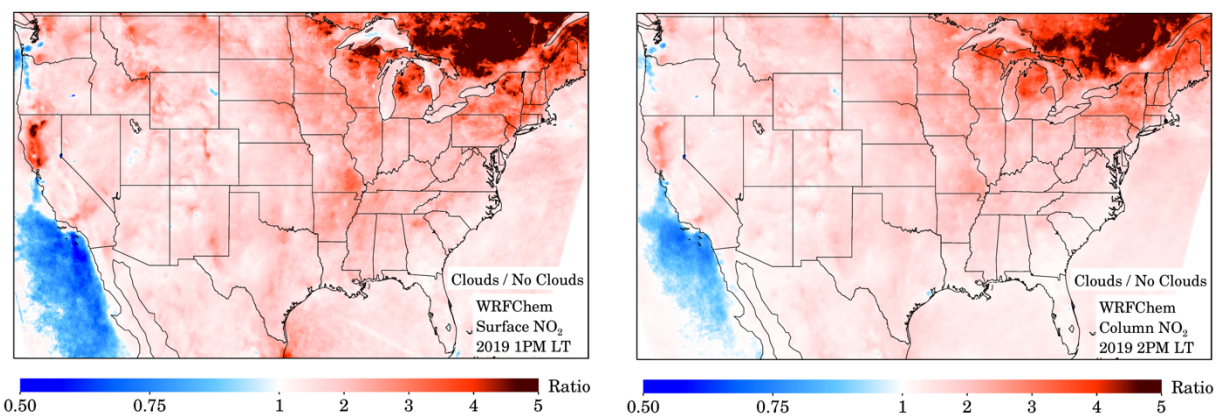


Figure 7. Ratio of the annualized surface NO₂ at 13:30 local time from WRF-Chem during cloudy and no cloud days. (Left) Surface NO₂ (Right) Tropospheric column NO₂.

3.5 Impacts of clouds on geostationary observations

Finally, we use provisional TEMPO NO_2 data, TROPOMI NO_2 data, and AQS NO_2 data from 2 August 2023 through 30 June 2024 to understand how the changes of NO_2 during clear and cloudy conditions may be altered at different hours of the day (Figure 8). In this analysis, the threshold between high quality and lower quality data for both satellite products is a cloud radiative fraction = 0.15. Any TEMPO NO_2 or TROPOMI NO_2 measurement with crf < 0.15 was assumed to be "clear sky", while all other measurements are assumed to be cloudy. Hours with low solar zenith angles (before 8:00 and after 16:00) have been excluded from this analysis. We find that the difference in surface NO_2 between clear and cloudy days is small in the early morning hours and increases throughout the day.

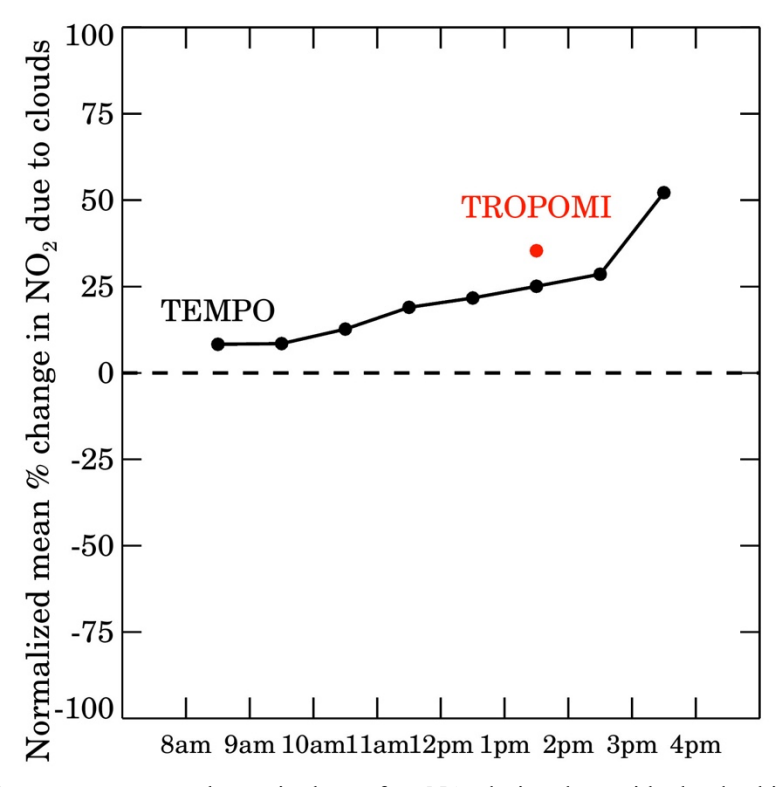


Figure 8. Normalized mean percentage change in the surface NO₂ during days with cloudy skies as opposed to days with clear skies. Red dot shows the mean percentage change using TROPOMI clouds as shown in Figure 2c. Black line uses the same procedure for Aug 2023 – June 2024 data and TEMPO cloud data.

Surface AQS NO₂ at 8:30 local time is +8.3% larger on cloudy days than clear sky days, while at 15:30 it is +52.2% larger. The calculated 13:30 difference in surface NO₂ between cloudy and clear sky days using TEMPO (+25.1%) is similar to the analogous value from TROPOMI (+35.4%). Differences between TEMPO and TROPOMI are expected because the cloud algorithms and instrument characteristics are different, even though the timeframe and cloud filter threshold used for this analysis are the same.

4 Discussion

In this project we quantify how NO₂ satellite data could be biased in estimating annualized surface NO₂ concentrations due to having high quality measurements only in the absence of clouds. We find that surface *in situ* NO₂ measurements are on average +17% on all days compared to restricting to clear sky days and +36% larger during cloudy days vs. clear sky days, with a wide distribution based on geographic region and proximity to roadway. Using the United States as a case study, we find the clear-sky bias to be largest in the Northeast U.S.; conversely, the clear-sky bias is smallest in the Southwest U.S. and near major roadways. In some areas of the urban Western U.S., Los Angeles and San Diego, we find that NO₂ is lower on cloudy days, but these instances are rare (13% of monitoring sites) and are driven by unique transport patterns on cloudy days. Transport patterns are a significant driver of the regional clear vs. cloudy sky differences of surface NO₂ concentrations. Although the analysis was computed for both TROPOMI and TEMPO data, it should be re-emphasized that the cloud algorithms

407 cloudy and clear conditions tend to be larger in the afternoon than morning is consistent with a hypothesis that active 408 photochemistry during periods of stronger afternoon sunlight would cause this change. 409 This work also highlights how NO₂ concentrations are different on days when satellite instruments are not acquiring 410 a valid measurement. Our initial hypothesis of NO2 being consistently larger on cloudy days was only partially 411 proven true. In many cases, surface NO₂ concentrations and column NO₂ are larger, but this is not always the case. 412 This project demonstrates the balancing act of the reduced NO₂ + OH sink and local climatological patterns (wind 413 speed/direction, PBL depth, etc.) driving surface NO₂ during cloudy conditions. Although one of the original goals 414 of this study was to better gap-fill satellite tropospheric vertical column NO₂ measurements in the presence of 415 clouds, ultimately, we were not comfortable doing this yet. Reliance on a model as a transfer standard to convert 416 surface concentrations into column concentrations exhibited too many biases under cloudy conditions. WRF-Chem 417 model simulations of surface NO2 suggest that the clear-sky bias in WRF-Chem is on average much larger than the observed clear-sky bias: +59% on cloudy days vs. clear days for the model, and +36% for the AQS data. We 418 419 hypothesized that errors in OH chemistry, NO2 recycling speeds, and PBL mixing depths could all be contributing to 420 this high bias. Future work should target these three research topics. Future work could also use a machine-learning 421 approach to account for some of these model biases. 422 Another consideration with the interpretation of satellite measurements is the impact of lightning NOx, wildfire 423 NOx, and aircraft NOx emissions, mostly staying aloft, which could be misinterpreted as surface NO2 424 enhancements. While lightning NOx and wildfire NOx emissions are often screened out when applying a cloud filter 425 because they occur in optically thick clouds/smoke, it is possible for the NO2 to remain aloft for several days after 426 the initial thunderstorm/fire and be observed during clear skies. An algorithm to detect and screen out downwind 427 NO₂ attributed to upwind lightning NOx and wildfire NOx emissions could be especially helpful. At minimum, care 428 should be taken during timeframes and regions where there are large pulses of these types of emissions, such as our 429 findings during summer. 430 In some ways, the chosen year 2019 was an ideal year to conduct the analysis because it preceded the 2020 global 431 pandemic and its nonlinear and lingering effects on air pollution. But in other ways, this year was less ideal because 432 TROPOMI pixel sizes changed in August 2019 from $7 \times 3.5 \text{ km}^2$ ($\sim 25 \text{ km}^2$) to $5.5 \times 3.5 \text{ km}^2$ ($\sim 19 \text{ km}^2$) The fraction 433 of clear-sky pixels likely increased by 1-2% after August 2019 as smaller pixel sizes can better "see around" 434 clouds (Krijger et al., 2007). This probably did not meaningfully affect our analysis but is nonetheless a caveat of 435 using 2019 data. 436 These results have repercussions for many applied studies that use satellite data to estimate surface NO₂ 437 concentrations or NOx emissions. First, for studies that estimate surface concentrations, it is important to ingest 438 surface NO₂ measurements during cloudy (and nighttime) conditions in some capacity in order to appropriately 439 estimate 24-hour concentrations; most studies already do this. If one were to use the clear-sky satellite data coupled 440 with only a chemical transport model as a transfer standard to convert the column measurement into a pseudo-

used by both instruments are different. However, the qualitative finding that surface NO2 differences between

surface "measurement", this would underestimate annualized NO2 concentration in most places. Unfortunately, there are many global regions with few or no surface measurements, so this is an important consideration when estimating surface NO₂ in these regions. But even if one were to ingest surface NO₂ during cloudy conditions, the spatial patterns of surface NO2 during cloudy conditions may be slightly different than implied by the clear-sky satellite data. For example, we find that NO2 surface concentrations under cloudy conditions are much larger in the Northeast U.S. than the Southwest U.S., and a cloud-free satellite map does not capture this. Second, for nitrogen oxide emissions estimates it is often assumed that anthropogenic emission rates are similar under cloudy and clear-sky conditions, but this is likely not the case in reality. Although we show that surface NO₂ concentrations are typically smaller under clear-skies, it is likely that anthropogenic NOx emissions are actually larger under regionwide clear-skies during summer and winter due to the moderating impact of clouds on surface temperature and subsequent impacts on heating-ventilation-air conditioning (HVAC) usage/emissions (Abel et al., 2017). If we were able to better independently estimate tropospheric vertical column NO₂ during cloudy conditions, perhaps this could be investigated in the future. Lastly, as satellite-derived NO₂ applications increase over the coming years, it is important to document its successes and shortcomings. We see this project as a first-step towards better accounting for the clear-sky bias of satellite NO2 data. While future NO2 applications may use geostationary data, such as TEMPO, which may suffer from a similar bias depending on the hour of the day, an advantage of geostationary satellite data is the ability to use multiple measurements per day before and just after the clouds. It might be possible to isolate a two-hour window (one with a cloud and one without) to get a better handle on the instantaneous versus long-term role of clouds affecting NO₂ concentrations. This work also highlights the critical role that chemical transport models can play in satellite NO₂ applications. Errors in the model assumptions can hamstring many NO₂ applications. For example, using a model to infer NO₂ during cloudy conditions in the lack of clear-sky satellite data would yield significant errors. Therefore, future work should concurrently focus on acquiring and using sub-orbital measurements to diagnose errors related in simulating NO₂ in chemical transport models, so that they can be used as more robust transfer standards.

441

442

443

444

445

446

447

448

449

450

451

452

453

454

455

456

457

458

459

460

461

462

463

464

- Data availability. TROPOMI NO₂ version 2.4 data (http://doi.org/10.5270/S5P-9bnp8q8) processed to 0.01° ×
- 467 0.01° resolution (http://doi.org/10.5067/MKJG22GUOD34) and TEMPO NO2 version 3 data
- 468 (http://doi.org/10.5067/IS-40e/TEMPO/NO2 L3.003) can be freely downloaded from NASA Earthdata. EPA AQS
- surface NO₂ data can be downloaded from pre-generated files:
- 470 https://ags.epa.gov/agsweb/airdata/download_files.html. ERA5 re-analysis hourly data on single levels
- 471 (http://doi.org/10.24381/cds.adbb2d47) can be downloaded from Copernicus Climate Data Store
- 472 (https://cds.climate.copernicus.eu/#!/home). NOAA SURFAD data can be downloaded from:
- 473 https://gml.noaa.gov/grad/surfrad/sitepage.html . Output from the WRF-Chem simulation is available upon request.
- 474 IDL code to process the data is available upon request.

475

- 476 Author contribution. D.G., A.C., S.K., and S.A. developed the project design. J.H. and C.L. set-up and conducted
- 477 the WRF-Chem simulations. D.G downloaded and processed the TROPOMI NO2, TEMPO NO2, ERA5, and
- 478 SURFRAD data and re-gridded all data to a standardized grid. M.O.N. helped to process the surface NO₂ data. D.G.
- 479 developed all figures for the manuscript and wrote the paper. All authors edited the manuscript.

480

Competing interests. The contact author has declared that none of the authors have any competing interests.

482

- 483 Acknowledgments. Preparation of this manuscript was funded by grants from the NOAA GeoXO program
- 484 (1305M323PNRMA0668) and the NASA Health and Air Quality Applied Sciences Team (HAQAST)
- 485 (80NSSC21K0511). NOAA Cooperative Agreement (NA17OAR4320101 and NA22OAR4320151) funded C. Lyu
- and J. He. The WRF-Chem simulation was supported by NOAA's High Performance Computing Program. The
- 487 authors would also like to thank Brian McDonald and Laura Judd for very helpful feedback during preparation of this
- 488 manuscript.

489

- 490 **Supporting Information.** The supporting information includes: 1) a spatial plot of the annual average of days with
- total cloud fraction less 0.5 as simulated by WRF-Chem during 8 AM, 1 PM, and 5 PM local time, 2) scatterplots of
- various 2019 annual averages of surface NO₂ and TROPOMI NO₂ measurements, 3) jNO₂ from WRF-Chem and an
- intercomparison with the NOAA SURFRAD network, 4) Tables of "cloudy vs. all days" and "all days vs. no
- 494 clouds" analogous to Table 1 which shows "cloudy vs. no clouds".

496

497	References
498 499 500	Abel, D. W., Holloway, T., Kladar, R. M., Meier, P., Ahl, D., Harkey, M., & Patz, J. (2017). Response of Power Plant Emissions to Ambient Temperature in the Eastern United States. <i>Environmental Science and Technology</i> , 51(10), 5838–5846. https://doi.org/10.1021/acs.est.6b06201
501 502	Acker, S. J., Holloway, T., & Harkey, M. K. (2025, February 13). Satellite Detection of NO2 Distributions and Comparison with Ground-Based Concentrations. <i>EGUsphere</i> . https://doi.org/10.5194/egusphere-2025-226
503 504 505	Anenberg, S. C., Mohegh, A., Goldberg, D. L., Kerr, G. H., Brauer, M., Burkart, K., et al. (2022). Long-term trends in urban NO2 concentrations and associated paediatric asthma incidence: estimates from global datasets. <i>The Lancet Planetary Health</i> , <i>6</i> (1), e49–e58. https://doi.org/10.1016/S2542-5196(21)00255-2
506 507 508	Bechle, M. J., Millet, D. B., & Marshall, J. D. (2015). National Spatiotemporal Exposure Surface for NO2: Monthly Scaling of a Satellite-Derived Land-Use Regression, 2000-2010. <i>Environmental Science and Technology</i> , 49(20), 12297–12305. https://doi.org/10.1021/acs.est.5b02882
509 510 511	Boersma, K. F., Eskes, H. J., Dirksen, R. J., Van Der A, R. J., Veefkind, J. P., Stammes, P., et al. (2011). An improved tropospheric NO2 column retrieval algorithm for the Ozone Monitoring Instrument. <i>Atmospheric Measurement Techniques</i> , 4(9), 1905–1928. https://doi.org/10.5194/amt-4-1905-2011
512 513 514	Burnett, R. T., Stieb, D., Brook, J. R., Cakmak, S., Dales, R., Raizenne, M., et al. (2004). Associations between short-term changes in nitrogen dioxide and mortality in Canadian cities. <i>Archives of Environmental Health</i> , 59(5), 228–236. https://doi.org/10.3200/AEOH.59.5.228-236
515 516 517	Busca, G., Lietti, L., Ramis, G., & Berti, F. (1998). Chemical and mechanistic aspects of the selective catalytic reduction of NO(x) by ammonia over oxide catalysts: A review. <i>Applied Catalysis B: Environmental</i> , 18(1–2), 1–36. https://doi.org/10.1016/S0926-3373(98)00040-X
518 519	Cao, E. L. (2023). National ground-level NO2 predictions via satellite imagery driven convolutional neural networks. <i>Frontiers in Environmental Science</i> , 11. https://doi.org/10.3389/fenvs.2023.1285471
520 521 522	Crippa, M., Guizzardi, D., Pisoni, E., Solazzo, E., Guion, A., Muntean, M., et al. (2021). Global anthropogenic emissions in urban areas: patterns, trends, and challenges. <i>Environmental Research Letters</i> , 16(7), 074033. https://doi.org/10.1088/1748-9326/AC00E2
523 524 525 526	Demetillo, M. A. G., Navarro, A., Knowles, K. K., Fields, K. P., Geddes, J. A., Nowlan, C. R., et al. (2020). Observing Nitrogen Dioxide Air Pollution Inequality Using High-Spatial-Resolution Remote Sensing Measurements in Houston, Texas. <i>Environmental Science & Technology</i> , <i>54</i> (16), 9882–9895. https://doi.org/10.1021/acs.est.0c01864
527 528	Dickerson, R. R., Anderson, D. C., & Ren, X. (2019). On the use of data from commercial NOx analyzers for air pollution studies. <i>Atmospheric Environment</i> , 214, 116873. https://doi.org/10.1016/j.atmosenv.2019.116873
529 530 531 532	Dressel, I. M., Demetillo, M. A. G., Judd, L. M., Janz, S. J., Fields, K. P., Sun, K., et al. (2022). Daily Satellite Observations of Nitrogen Dioxide Air Pollution Inequality in New York City, New York and Newark, New Jersey: Evaluation and Application. <i>Environmental Science and Technology</i> , 2022. https://doi.org/10.1021/ACS.EST.2C02828/ASSET/IMAGES/LARGE/ES2C02828_0006.JPEG
533 534	Duncan, B. N., Anderson, D. C., Fiore, A. M., Joiner, J., Krotkov, N. A., Li, C., et al. (2024). Opinion: Beyond global means – novel space-based approaches to indirectly constrain the concentrations of and trends and

535 536	variations in the tropospheric hydroxyl radical (OH). <i>Atmospheric Chemistry and Physics</i> , 24(22), 13001–13023. https://doi.org/10.5194/acp-24-13001-2024
537 538	Eskes, H., van Geffen, J., Boersma, F., Eichman, K., Apituley, A., Pedergnana, M., et al. (2022). Sentinel-5 precursor/TROPOMI Level 2 Product User Manual Nitrogendioxide.
539	de Foy, B., Krotkov, N. A., Bei, N., Herndon, S. C., Huey, L. G., Martínez, AP., et al. (2009). Hit from both sides:
540	tracking industrial and volcanic plumes in Mexico City with surface measurements and OMI SO2 retrievals
541	during the MILAGRO field campaign. Atmospheric Chemistry and Physics, 9(24), 9599–9617.
542	https://doi.org/10.5194/acp-9-9599-2009
543	Geddes, J. A., Murphy, J. G., O'Brien, J. M., & Celarier, E. A. (2012). Biases in long-term NO2 averages inferred
544	from satellite observations due to cloud selection criteria. Remote Sensing of Environment, 124(2), 210–216.
545	https://doi.org/10.1016/j.rse.2012.05.008
546 547	van Geffen, J. (2016). TROPOMI ATBD of the total and tropospheric NO2 data products, (2). Retrieved from https://sentinel.esa.int/documents/247904/2476257/Sentinel-5P-TROPOMI-ATBD-NO2-data-products
548	van Geffen, J., Boersma, K. F., Eskes, H. J., Sneep, M., ter Linden, M., Zara, M., & Veefkind, J. P. (2020). S5P
549	TROPOMI NO2 slant column retrieval: method, stability, uncertainties and comparisons with OMI.
550	Atmospheric Measurement Techniques, 13(3), 1315–1335. https://doi.org/10.5194/amt-13-1315-2020
551	van Geffen, J., Eskes, H. J., Compernolle, S., Pinardi, G., Verhoelst, T., Lambert, JC., et al. (2021). Sentinel-5P
552	TROPOMI NO2 retrieval: impact of version v2.2 improvements and comparisons with OMI and ground-based
553	data. Atmospheric Measurement Techniques, 15(7), 2037–2060. https://doi.org/10.5194/AMT-15-2037-2022
554	Ghahremanloo, M., Lops, Y., Choi, Y., & Yeganeh, B. (2021). Deep Learning Estimation of Daily Ground-Level
555	NO2 Concentrations From Remote Sensing Data. Journal of Geophysical Research: Atmospheres, 126(21),
556	e2021JD034925. https://doi.org/10.1029/2021JD034925
557	Ghahremanloo, M., Lops, Y., Choi, Y., Mousavinezhad, S., & Jung, J. (2023). A Coupled Deep Learning Model for
558	Estimating Surface NO2 Levels from Remote Sensing Data: 15-Year Study Over the Contiguous United
559	States. Journal of Geophysical Research: Atmospheres, e2022JD037010.
560	https://doi.org/10.1029/2022JD037010
561	Glissenaar, I., Folkert Boersma, K., Anglou, I., Rijsdijk, P., Verhoelst, T., Compernolle, S., et al. (2025). TROPOMI
562	Level 3 tropospheric NO2 Dataset with Advanced Uncertainty Analysis from the ESA CCI+ ECV Precursor
563	Project. EGUsphere. https://doi.org/10.21944/CCI-NO2-TROPOMI-L3
564	Goldberg, D. L., Anenberg, S. C., Kerr, G. H., Mohegh, A., Lu, Z., & Streets, D. G. (2021). TROPOMI NO2 in the
565	United States: A Detailed Look at the Annual Averages, Weekly Cycles, Effects of Temperature, and
566	Correlation With Surface NO 2 Concentrations. Earth's Future, 9(4), e2020EF001665.
567	https://doi.org/10.1029/2020EF001665
568	Goldberg, D. L., Harkey, M., de Foy, B., Judd, L., Johnson, J., Yarwood, G., & Holloway, T. (2022). Evaluating
569	NOx emissions and their effect on O3 production in Texas using TROPOMI NO2 and HCHO. Atmospheric
570	Chemistry and Physics, 22(16), 10875–10900. https://doi.org/10.5194/acp-22-10875-2022
571	Goldberg, D. L., Tao, M., Kerr, G. H., Ma, S., Tong, D. Q., Fiore, A. M., et al. (2024). Evaluating the spatial
572	patterns of U.S. urban NOx emissions using TROPOMI NO2. Remote Sensing of Environment, 300, 113917.
573	https://doi.org/10.1016/j.rse.2023.113917

- Harkey, M., & Holloway, T. (2024). Simulated Surface-Column NO2 Connections for Satellite Applications.
- 575 Journal of Geophysical Research: Atmospheres, 129(21). https://doi.org/10.1029/2024JD041912
- He, J., Harkins, C., O'Dell, K., Li, M., Francoeur, C., Aikin, K. C., et al. (2024). COVID-19 perturbation on US air
- quality and human health impact assessment. PNAS Nexus, 3(1). https://doi.org/10.1093/pnasnexus/pgad483
- He, M. Z., Kinney, P. L., Li, T., Chen, C., Sun, Q., Ban, J., et al. (2020). Short- and intermediate-term exposure to
- NO2 and mortality: A multi-county analysis in China. *Environmental Pollution*, 261, 114165.
- 580 https://doi.org/10.1016/j.envpol.2020.114165
- 581 Health Effects Institute. (2022). Systematic Review and Meta-analysis of Selected Health Effects of Long-Term
- 582 Exposure to Traffic-Related Air Poll. Retrieved from https://www.healtheffects.org/system/files/hei-special-
- report-23-executive-summary_0.pdf
- Hegarty, J. D., Lewis, J., McGrath-Spangler, E. L., Henderson, J., Scarino, A. J., DeCola, P., et al. (2018). Analysis
- of the Planetary Boundary Layer Height during DISCOVER-AQ Baltimore—Washington, D.C., with Lidar and
- High-Resolution WRF Modeling. *Journal of Applied Meteorology and Climatology*, *57*(11), 2679–2696.
- 587 https://doi.org/10.1175/JAMC-D-18-0014.1
- Hersbach, H., Bell, B., Berrisford, P., Hirahara, S., Horányi, A., Muñoz-Sabater, J., et al. (2020). The ERA5 global
- 589 reanalysis. Quarterly Journal of the Royal Meteorological Society, 146(730), 1999–2049.
- 590 https://doi.org/10.1002/qj.3803
- Jin, X., Zhu, Q., & Cohen, R. C. (2021). Direct estimates of biomass burning NOx emissions and lifetimes using
- daily observations from TROPOMI. Atmospheric Chemistry and Physics, 21(20), 15569–15587.
- 593 https://doi.org/10.5194/acp-21-15569-2021
- Kebabian, P. L., Wood, E. C., Herndon, S. C., & Freedman, A. (2008). A practical alternative to
- chemiluminescence-based detection of nitrogen dioxide: Cavity attenuated phase shift spectroscopy.
- 596 Environmental Science and Technology, 42(16), 6040–6045. https://doi.org/10.1021/es703204j
- Kelly, K. E., Whitaker, J., Petty, A., Widmer, C., Dybwad, A., Sleeth, D., et al. (2017). Ambient and laboratory
- 598 evaluation of a low-cost particulate matter sensor. *Environmental Pollution*, 221, 491–500.
- 599 https://doi.org/10.1016/j.envpol.2016.12.039
- 600 Kenagy, H. S., Sparks, T. L., Ebben, C. J., Wooldrige, P. J., Lopez-Hilfiker, F. D., Lee, B. H., et al. (2018). NOx
- 601 Lifetime and NOy Partitioning During WINTER. Journal of Geophysical Research: Atmospheres, 123(17),
- 602 9813–9827. https://doi.org/10.1029/2018JD028736
- Kerr, G. H., Goldberg, D. L., Harris, M. H., Henderson, B. H., Hystad, P., Roy, A., & Anenberg, S. C. (2023).
- 604 Ethnoracial Disparities in Nitrogen Dioxide Pollution in the United States: Comparing Data Sets from
- Satellites, Models, and Monitors. *Environmental Science & Technology*.
- 606 https://doi.org/10.1021/acs.est.3c03999
- Khreis, H., Kelly, C., Tate, J., Parslow, R., Lucas, K., & Nieuwenhuijsen, M. (2017). Exposure to traffic-related air
- pollution and risk of development of childhood asthma: A systematic review and meta-analysis. *Environment*
- 609 International, 100, 1–31. https://doi.org/10.1016/j.envint.2016.11.012
- 610 Kim, E. J., Holloway, T., Kokandakar, A., Harkey, M., Elkins, S., Goldberg, D. L., & Heck, C. (2024). A
- 611 Comparison of Regression Methods for Inferring Near-Surface NO 2 With Satellite Data. *Journal of*
- 612 Geophysical Research: Atmospheres, 129(16). https://doi.org/10.1029/2024JD040906

- Koltsakis, G., & Stamatelos, A. (1997). Catalytic automotive exhaust aftertreatment. *Progress in Energy and Combustion Science*, 22(1), 1, 20, https://doi.org/10.1016/s0260.1285(07)00002.8
- 614 Combustion Science, 23(1), 1–39. https://doi.org/10.1016/s0360-1285(97)00003-8
- Krijger, J. M., Van Weele, M., Aben, I., & Frey, R. (2007). Atmospheric Chemistry and Physics Technical Note:
- The effect of sensor resolution on the number of cloud-free observations from space. Atmos. Chem. Phys (Vol.
- 7). Retrieved from www.atmos-chem-phys.net/7/2881/2007/
- Kuhn, L., Beirle, S., Kumar, V., Osipov, S., Pozzer, A., Bösch, T., et al. (2024). On the influence of vertical mixing,
- 619 boundary layer schemes, and temporal emission profiles on tropospheric NO2 in WRF-Chem comparisons
- 620 to in situ, satellite, and MAX-DOAS observations. *Atmospheric Chemistry and Physics*, 24(1), 185–217.
- 621 https://doi.org/10.5194/acp-24-185-2024
- Lambert, J.-C., Claas, J., Stein-Zweers, D., Ludewig, A., Loyola, D., Sneep, M., & Dehn, A. (2023). *Quarterly*
- 623 Validation Report of the Copernicus Sentinel-5 Precursor Operational Data Products #19.
- 624 Lamsal, L. N., Martin, R. V., van Donkelaar, A., Steinbacher, M., Celarier, E. A., Bucsela, E. J., et al. (2008).
- Ground-level nitrogen dioxide concentrations inferred from the satellite-borne Ozone Monitoring Instrument.
- Journal of Geophysical Research Atmospheres, 113(16), 1–15. https://doi.org/10.1029/2007JD009235
- 627 Larkin, A., Anenberg, S., Goldberg, D. L., Mohegh, A., Brauer, M., & Hystad, P. (2023). A global spatial-temporal
- land use regression model for nitrogen dioxide air pollution. Frontiers in Environmental Science, 11, 484.
- 629 https://doi.org/10.3389/FENVS.2023.1125979
- Laughner, J. L., & Cohen, R. C. (2019). Direct observation of changing NOx lifetime in North American cities.
- 631 *Science*, 366(6466), 723–727. https://doi.org/10.1126/science.aax6832
- 632 Levelt, P. F., Joiner, J., Tamminen, J., Veefkind, J. P., Bhartia, P. K., Zweers, D. C. S., et al. (2018). The Ozone
- Monitoring Instrument: Overview of 14 years in space. Atmospheric Chemistry and Physics, 18(8), 5699–
- 634 5745. https://doi.org/10.5194/acp-18-5699-2018
- Lin, M., Horowitz, L. W., Hu, L., & Permar, W. (2024). Reactive Nitrogen Partitioning Enhances the Contribution
- of Canadian Wildfire Plumes to US Ozone Air Quality. *Geophysical Research Letters*, 51(15).
- https://doi.org/10.1029/2024GL109369
- 638 Liu, F., Beirle, S., Zhang, Q., Dörner, S., He, K., & Wagner, T. (2016). NOx lifetimes and emissions of cities and
- power plants in polluted background estimated by satellite observations. Atmospheric Chemistry and Physics,
- 640 16(8), 5283–5298. https://doi.org/10.5194/acp-16-5283-2016
- 641 Liu, S., Valks, P., Pinardi, G., Xu, J., Chan, K. L., Argyrouli, A., et al. (2021). An improved TROPOMI
- tropospheric NO2 research product over Europe. *Atmospheric Measurement Techniques*, 14(11), 7297–7327.
- 643 https://doi.org/10.5194/amt-14-7297-2021
- 644 Liu, X., Wang, Y., Wasti, S., Li, W., Soleimanian, E., Flynn, J., et al. (2023). Evaluating WRF-GC v2.0 predictions
- of boundary layer height and vertical ozone profile during the 2021 TRACER-AQ campaign in Houston,
- Texas. Geoscientific Model Development, 16(18), 5493–5514. https://doi.org/10.5194/gmd-16-5493-2023
- Lorente, A., Folkert Boersma, K., Yu, H., Dörner, S., Hilboll, A., Richter, A., et al. (2017). Structural uncertainty in
- air mass factor calculation for NO2 and HCHO satellite retrievals. Atmospheric Measurement Techniques,
- 649 10(3), 759–782. https://doi.org/10.5194/amt-10-759-2017

- Martin, R. V., Brauer, M., van Donkelaar, A., Shaddick, G., Narain, U., & Dey, S. (2019). No one knows which city
- has the highest concentration of fine particulate matter. Atmospheric Environment: X, 100040.
- https://doi.org/10.1016/J.AEAOA.2019.100040
- Maruhashi, J., Mertens, M., Grewe, V., & Dedoussi, I. C. (2024). A multi-method assessment of the regional
- sensitivities between flight altitude and short-term O3 climate warming from aircraft NOx emissions.
- 655 Environmental Research Letters. https://doi.org/10.1088/1748-9326/ad376a
- Nault, B. A., Laughner, J. L., Wooldridge, P. J., Crounse, J. D., Dibb, J., Diskin, G., et al. (2017). Lightning NOx
- Emissions: Reconciling Measured and Modeled Estimates With Updated NOx Chemistry. *Geophysical*
- 658 Research Letters, 44(18), 9479–9488. https://doi.org/10.1002/2017GL074436
- Nawaz, M. O., Goldberg, D. L., Kerr, G. H., & Anenberg, S. C. (2025). TROPOMI Satellite Data Reshape NO2 Air
- Pollution Land-Use Regression Modeling Capabilities in the United States. ACS ES&T Air.
- https://doi.org/10.1021/acsestair.4c00153
- Palmer, P. I., Jacob, D. J., Chance, K. V., Martin, R. V., Spurr, R. J. D., Kurosu, T. P., et al. (2001). Air mass factor
- formulation for spectroscopic measurements from satellites: Application to formaldehyde retrievals from the
- Global Ozone Monitoring Experiment. Journal of Geophysical Research: Atmospheres, 106(D13), 14539–
- 665 14550. https://doi.org/10.1029/2000JD900772
- Platt, U. (1994). Differential Optical Absorption Spectroscopy (DOAS). In *Air monitoring by spectroscopic techniques* (p. 531). Wiley-IEEE.
- Poraicu, C., Müller, J.-F., Stavrakou, T., Fonteyn, D., Tack, F., Deutsch, F., et al. (2023). Cross-evaluating WRF-
- 669 Chem v4.1.2, TROPOMI, APEX, and in situ NO2 measurements over Antwerp, Belgium. Geosci. Model Dev,
- 670 16, 479–508. https://doi.org/10.5194/gmd-16-479-2023
- Rijsdijk, P., Eskes, H., Dingemans, A., Boersma, K. F., Sekiya, T., Miyazaki, K., & Houweling, S. (2025).
- Quantifying uncertainties in satellite NO2 superobservations for data assimilation and model evaluation.
- 673 Geoscientific Model Development, 18(2), 483–509. https://doi.org/10.5194/gmd-18-483-2025
- Ryu, Y. H., Hodzic, A., Barre, J., Descombes, G., & Minnis, P. (2018). Quantifying errors in surface ozone
- predictions associated with clouds over the CONUS: A WRF-Chem modeling study using satellite cloud
- 676 retrievals. Atmospheric Chemistry and Physics, 18(10), 7509–7525. https://doi.org/10.5194/acp-18-7509-2018
- 677 Sarwar, G., Hogrefe, C., Henderson, B. H., Mathur, R., Gilliam, R., Callaghan, A. B., et al. (2024). Impact of
- particulate nitrate photolysis on air quality over the Northern Hemisphere. Science of The Total Environment,
- 679 917, 170406, https://doi.org/10.1016/j.scitotenv.2024.170406
- 680 Shah, V., Jacob, D. J., Li, K., Silvern, R. F., Zhai, S., Liu, M., et al. (2020). Effect of changing NOx lifetime on the
- seasonality and long-term trends of satellite-observed tropospheric NO2 columns over China. *Atmospheric*
- 682 Chemistry and Physics Discussions, 20(3), 1483–1495. https://doi.org/10.5194/acp-2019-670
- 683 Shah, V., Keller, C. A., Knowland, K. E., Christiansen, A., Hu, L., Wang, H., et al. (2024). Particulate Nitrate
- Photolysis as a Possible Driver of Rising Tropospheric Ozone. *Geophysical Research Letters*, 51(5).
- 685 https://doi.org/10.1029/2023GL107980
- Shetty, S., Schneider, P., Stebel, K., David Hamer, P., Kylling, A., & Koren Berntsen, T. (2024). Estimating surface
- NO2 concentrations over Europe using Sentinel-5P TROPOMI observations and Machine Learning. *Remote*
- 688 Sensing of Environment, 312, 114321. https://doi.org/10.1016/j.rse.2024.114321

689 Sullivan, D. M., & Krupnick, A. (2018). Using Satellite Data to Fill the Gaps in the US Air Pollution Monitoring 690 Network. NW. Retrieved from https://www.rff.org/publications/working-papers/using-satellite-data-to-fill-the-691 gaps-in-the-us-air-pollution-monitoring-network/ 692 Sun, K., Zhu, L., Cady-Pereira, K. E., Chan Miller, C., Chance, K. V., Clarisse, L., et al. (2018). A physics-based 693 approach to oversample multi-satellite, multi-species observations to a common grid. Atmospheric 694 Measurement Techniques Discussions, 11(12), 1–30. https://doi.org/10.5194/amt-2018-253 695 Sun, W., Tack, F., Clarisse, L., Schneider, R., Stavrakou, T., & Van Roozendael, M. (2024), Inferring Surface NO2 696 Over Western Europe: A Machine Learning Approach With Uncertainty Quantification. Journal of 697 Geophysical Research: Atmospheres, 129(20). https://doi.org/10.1029/2023JD040676 698 Thornton, J. A., Wooldridge, P. J., & Cohen, R. C. (2000). Atmospheric NO2: In Situ Laser-Induced Fluorescence 699 Detection at Parts per Trillion Mixing Ratios. Analytical Chemistry, 72(3), 528–539. 700 https://doi.org/10.1021/ac9908905 701 Vandaele, A. C., Hermans, C., Simon, P. C., Carleer, M., Colin, R., Fally, S., et al. (1998). Measurements of the 702 NO2 absorption cross-section from 42 000 cm-1 to 10 000 cm-1 (238-1000 nm) at 220 K and 294 K. Journal 703 of Quantitative Spectroscopy and Radiative Transfer, 59(3-5), 171-184. https://doi.org/10.1016/S0022-704 4073(97)00168-4 705 Veefkind, J. P., Aben, I., McMullan, K., Förster, H., de Vries, J., Otter, G., et al. (2012). TROPOMI on the ESA 706 Sentinel-5 Precursor: A GMES mission for global observations of the atmospheric composition for climate, air 707 quality and ozone layer applications. Remote Sensing of Environment, 120(2012), 70-83. 708 https://doi.org/10.1016/j.rse.2011.09.027 709 Zare, A., Romer, P. S., Nguyen, T., Keutsch, F. N., Skog, K., & Cohen, R. C. (2018). A comprehensive organic 710 nitrate chemistry: Insights into the lifetime of atmospheric organic nitrates. Atmospheric Chemistry and 711 Physics, 18(20), 15419–15436. https://doi.org/10.5194/acp-18-15419-2018 712 713